Ultramicroscopy 119 (2012) 51–56

Contents lists available at SciVerse ScienceDirect

Ultramicroscopy

journal homepage: www.elsevier.com/locate/ultramic

Localization of inelastic electron scattering in the low-loss energy regime ☆

Wu Zhou [a,b,*], Stephen J. Pennycook [a,b], Juan-Carlos Idrobo [a,b,**]

[a] Materials Science and Technology Division, Oak Ridge National Laboratory, Oak Ridge, TN 37831, USA
[b] Department of Physics and Astronomy, Vanderbilt University, Nashville, TN 37235, USA

ARTICLE INFO

Available online 23 November 2011

Keywords:
Delocalization
Low loss
Plasmon
EELS
Spatial resolution
STEM
Graphene

ABSTRACT

The spatial resolution and contrast level in electron energy-loss spectroscopy (EELS) imaging depend on the delocalization of the inelastic electron scattering cross sections. Theoretical calculations within the dipole approximation provide the lower limit for the delocalization of low loss signals, and suggest that atomic resolution EELS imaging in the low loss energy regime (< 50 eV) should be possible. Here, we directly measure the localization of the inelastic electron scattering at different energy loss in the low loss regime using a clean open edge of monolayer graphene. Our results demonstrate that the delocalization depends both on the energy loss and the specific electron excitation mode contributing to the energy loss. While the plasmons are delocalized over 1.2 nm, sub-nm enhancement is observed at the edge for the low-loss signal at 11 eV, indicating the possible formation of a one-dimensional plasmon (or inter-band transition) at the edge of monolayer graphene. Our results also suggest that if the initial states or final states are atomically localized, atomic resolution EELS imaging could be obtained even in the low loss region of the spectra.

© 2011 Elsevier B.V. All rights reserved.

1. Introduction

Inelastic scattering of a fast electron beam with a specimen forms the basis of electron energy-loss spectroscopy (EELS) [1] in electron microscopy, and provides unique information for the chemical nature and electronic structure of the specimen atoms with a spatial resolution that cannot be obtained by other means. With the development of aberration correction techniques and new instrumentations in electron microscopy, we are now in an era where materials can be studied atom by atom. From a fundamental point of view, it is, therefore, desirable to extract all the useful information contained in the inelastic electron scattering events, at the atomic scale, which raises the issue of the degree of localization of the EELS cross-sections at different energy ranges. In this paper, we examine the localization of collective (plasmon) and single particle EELS excitations using a test sample of monolayer graphene.

With the exception of thermal diffuse scattering, low loss inelastic electron scattering is generally considered to be delocalized in space compared to elastic scattering, and this delocalized nature imposes a physical limit on the spatial resolution that can be obtained with STEM-EELS imaging and energy filtered TEM imaging. The localization of the inelastic scattering can be viewed as the region that contains considerable overlap of the initial- and final-state wave functions [1–3], and in a classical model, the degree of localization generally increases with increasing energy loss [1]. The last point has been demonstrated by many aberration-corrected STEM-EELS imaging studies using the core-loss region of the spectra, which involves the excitation of highly localized inner shell electrons. In this case, the high energy loss signals are localized at the atomic positions, and the chemical identity, oxidation state and binding characters of individual atoms and atomic columns can be mapped out in two-dimensional projection with atomic resolution [4–10]. In contrast, atomic resolution EELS imaging using the low loss region of the spectra, which contains information about the optical response of materials such as band gaps, has not yet been achieved mainly due to the delocalization of the valence- and empty-states contributing to the low energy excitations.

Many attempts have been made, both experimentally and theoretically, to estimate the delocalization of inelastic electron scattering in the low loss region of the spectra [11–23], which can be described by the width of the real-space distribution of scattering probability, also called the point-spread function (PSF) assuming point scattering objects. The PSF for low loss signals typically has a sharp central peak and extended tails. Therefore, several parameters are commonly used to describe the shape of PSF, including the full-width at half maximum (FWHM), full-width at tenth maximum (FWTM) and width containing 50%

☆ In memoriam Professor Gertrude Rempfer on the occasion of her 100th birthday.

* Corresponding author. Tel.: +1 484 695 0885.
** Corresponding author.
E-mail addresses: wu.zhou@vanderbilt.edu (W. Zhou), idrobojc@ornl.gov (J.-C. Idrobo).

0304-3991/$ - see front matter © 2011 Elsevier B.V. All rights reserved.
doi:10.1016/j.ultramic.2011.11.013

or 80% of the total scattering intensity (d_{50} or d_{80}). Some of the important results are summarized in the new edition of Egerton's book [1]. In particular, theoretical calculations within the dipole approximation [12–14,19,22] suggest the PSFs in the energy loss range of 0 to 100 eV tend to have a constant FWHM, close to the size of the electron probe [19,22]; while the d_{80} values increase substantially as the energy loss decreases [19,22]. This seems to suggest that 2D atomic resolution EELS imaging can be feasibly obtained using the low loss region of the spectra, even though the increased d_{80} would result in a decrease in lattice contrast level. However, the fact is that atomic resolution imaging in the low loss region (with energy loss lower than ~100 eV, in the lack of core edges) has not yet been achieved. Accurate experimental measurement of the delocalization of inelastic electron scattering with low energy loss is, therefore, a desirable step towards the realization of 2D atomic resolution imaging with the low loss region of the spectra. If proved feasible, such low loss imaging would, in principle, allow the study of optical properties of materials with unprecedented spatial resolution.

In this study, we measure the inelastic scattering cross-section (intensity) as a function of distance from a clean open edge of monolayer graphene via EELS line scans, which allows us to quantitatively compare the delocalization of inelastic scattering cross-sections at different energy losses. Our results demonstrate that the delocalization depends both on the energy loss and the specific electron excitation mode contributing to the energy loss function. We also observe a sub-nanometer enhancement for the low-loss signal at 11 eV at the edge of graphene, arising from a new one-dimensional edge plasmon or inter-band transition mode. Our results indicate that full quantum mechanical calculations are needed in order to quantitatively predict the delocalization of specific inelastic scattering events [24]. Atomic resolution EELS imaging can, in principle, be obtained even in the low loss region of the spectra if the initial states or final states are atomically localized in the material.

2. Experiments

The major difficulties of experimental measurement of the delocalization of the inelastic cross-sections arise from the low signal to noise ratio, stability of the instrument and uncertainties in the shape of the sample [19]. The first two can be overcome, to some extent, by carefully adjusting the experimental settings. We measured the delocalization of the EELS signals in the low loss region using EELS line scans. The EELS experiments were performed with a Nion UltraSTEM, a dedicated STEM equipped with a cold field emission electron source and a corrector of third and fifth order aberrations, operating at 60 kV accelerating voltage [8]. With the new design of highly stable lens system and stage, atomic resolution imaging and core-loss edge mapping can be routinely performed on this instrument [8]. After aberration correction, this microscope is capable of providing a probe close to 1 Å diameter with a current of ~110 pA (Fig. 1).

EEL spectra were collected using a Gatan Enfina spectrometer, with an energy resolution of 0.5 eV for 0.1 eV/channel energy dispersion. The convergence semi-angle for the incident probe was ~30 mrad, which is kept unchanged in all the data sets. Several collection semi-angle settings in the spectrometer were used in our experiments, specifically 15 mrad, 35 mrad, 48 mrad and 76 mrad. During the EELS line scans, ADF signals were collected simultaneously from the ~86 to 200 mrad half-angle range, without sub-pixel scanning. A total of 800 or 900 spectra were collected for each line scan with pixel size of~0.3 Å. Dwell times of 0.08 s/pixel or 0.1 s/pixel were used during the line scans. For each line scan, unprocessed EEL spectra were collected under identical experimental settings with the electron beam on and off. Dark current subtraction and gain normalization were performed during the analysis of the data. This collection scheme helps to reduce the noise level of the resultant data sets. The high probe current and long dwell time settings also help to increase the signal-to-noise level in our measurements.

We used a clean open edge of monolayer graphene as the perfect edge for the delocalization measurement. As shown in Fig. 2, the EELS line scans were collected as the probe was brought from the graphene layer, which is only one atom thick, into the vacuum. When the line scan crosses the open graphene edge, the peak position of the last carbon atom unambiguously defines the position of the specimen edge. Using such an open graphene edge we can effectively eliminate any uncertainty in the shape of the sample.

Since we are measuring the delocalization from line scans on an edge sample, the point spread function (PSF), in this case, refers to the decay of the low loss signal from the graphene edge into vacuum. The shape of the PSF is described by the width from the graphene edge to half-maximum (WHM) and tenth-maximum (WTM) of the one-dimensional intensity profile, and the distance containing 50% or 80% of the total scattering (d_{50} or d_{80}). Note, all our measurements were performed under 60 kV. The low incident beam energy is expected to give a smaller degree of delocalization for inelastic scattering as compared with measurements/calculations performed under higher incident beam energy [1,19,23]. In a classical approximation, the d_{50} value follows a dependence on incident beam energy as $d_{50} \approx 0.8\lambda(E_0/E)^{3/4}$ [1,23],

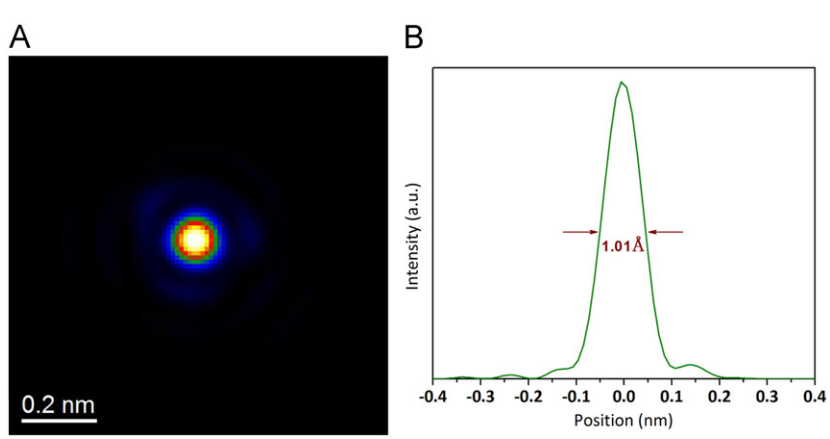

Fig. 1. Simulated electron probe with the aberration coefficients measured during the experiment. (A) Two dimensional probe intensity distribution. (B) Intensity profile along the horizontal section of the probe. The electron probe had a FWHM of ~1.01 Å, and a measured current of~110 pA.

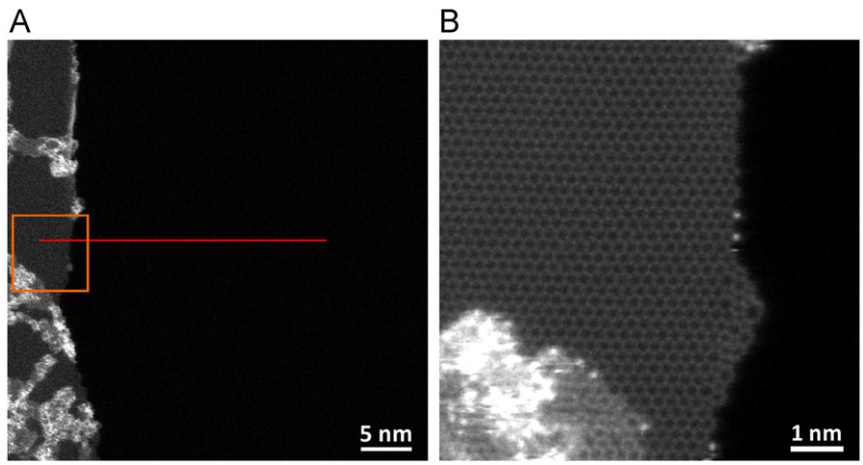

Fig. 2. ADF-STEM images of an open edge of monolayer graphene used for the measurement of the delocalization of the inelastic cross-section in the low energy loss range. EELS line scans were collected along the red line as indicated in Figure A. A closer view of the atomic structure of the open edge of monolayer graphene highlighted by the orange square is shown in B. (For interpretation of the references to color in this figure legend, the reader is referred to the web version of this article.)

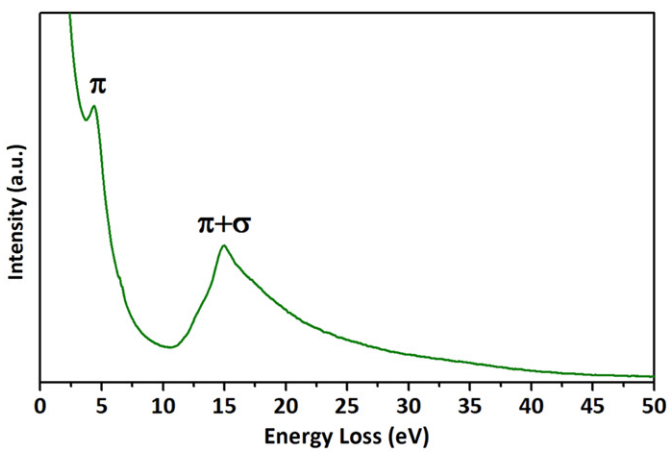

Fig. 3. Typical low loss spectrum from monolayer graphene showing the presence of π and $\pi+\sigma$ plasmon peaks at $\sim$4.5 and 15 eV, respectively.

where E is the energy loss, E_0 is the incident beam energy and λ is the wavelength for the incident electron beam, which is also a function of E_0.

3. Results and discussions

A typical low loss spectrum from monolayer graphene is shown in Fig. 3. Two main absorption peaks at $\sim$4.5 and 15 eV, commonly referred as the π and $\pi+\sigma$ surface plasmons [25], can be observed. Apart from these two plasmon peaks, no other distinct strong excitation can be observed in the low loss regime ($<$100 eV). The experimental measurement of inelastic scattering intensity as a function of distance from the edge of the monolayer graphene along the line scan is shown in Fig. 4. The pixel size in each of the line scans was calibrated based on the fast Fourier transform (FFT) of the graphene lattice in the corresponding survey ADF images. For an energy loss smaller than 50 eV, the intensity was integrated over a 1 eV energy window; while a 5 eV energy window was used for an energy loss higher than 50 eV in order to increase the signal-to-noise ratio. The integrated EELS intensity was normalized, for comparison purpose, such that the intensity at the edge position is set as 1, and the noise level was set to 0. As shown in Fig. 4A, at low energy loss, especially for the π and $\pi+\sigma$ plasmon peaks at $\sim$4.5 and 15 eV, respectively, the EELS signal is highly delocalized. The PSF of the inelastic scattering signals at this energy loss region ($<$25 eV) has a WHM much larger than the FWHM of the electron probe, and the tail of the PSF can extend for more than 10 nm away from the graphene edge. The WHM of the PSF displays a drastic drop at energy losses above the $\pi+\sigma$ plasmon peak, and decreases gradually as the energy loss increases, approaching the FWHM of the electron probe at$\sim$100 eV. Similar behavior can be observed for the tail of the PSF.

In order to quantify the delocalization of the EELS signal at different energy losses, we measure the WHM, WTM, d_{50} and d_{80} values of the PSF as a function of energy loss. While the WHM and d_{50} measurements are quite robust to the noise level, noise at the tail of the PSF induces relatively larger error in the measurement of WTM and d_{80}. Notice at large distance from the graphene edge, the intensity of the signal follows an exponential decay. We, therefore, fit the experimental data at the PSF tail (starting from an intensity of $\sim$10% with respect to the maximum) with exponential decaying functions, and use the fitted data as the new PSF tail for the measurement of WTM, d_{50} and d_{80} values that are summarized in Fig. 5. Away from the two plasmon peaks, i.e. at an energy loss higher than 25 eV where no strong characteristic excitations are present, our experimental results are qualitatively in agreement with previous theoretical calculations within the dipole approximation [19,22]. Specifically, the WHM of the PSF in this energy loss range is only slightly worse than that of the incident electron probe, and depends weakly on the energy loss. The delocalization effect in this energy loss range is mainly reflected on the large tail of the PSF, which broadens at lower energy loss as shown by the increasing WTM and d_{80} values. For EELS imaging, this large tail would result in a decrease in lattice contrast. However, opposite to the semi-classical model, which predicts constant FWHM and FWTM at small energy loss ($<$25 eV) [19,22], there is a drastic increase in the WHM value and significant broadening in the tail of the PSF for the two graphene plasmon peaks at $\sim$4.5 and 15 eV. This rapid increase in delocalization cannot be expected from a simple dependence on the energy loss alone, and is most likely related to the specific electronic excitations that contribute to the two plasmon peaks. We further show in Fig. 6 that the delocalization behavior of the plasmon at 15 eV is not particularly sensitive to the collection angle settings for collection angles larger than the convergence angle, while the degree of delocalization increases slightly for

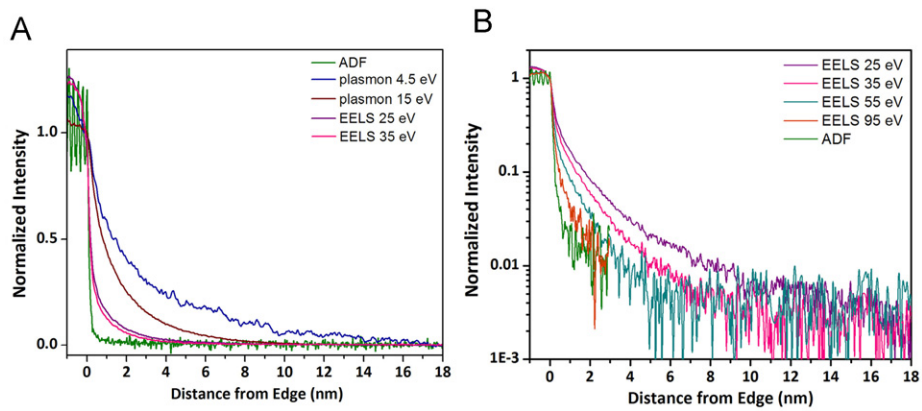

Fig. 4. Experimental measurement of the inelastic scattering intensity (normalized, along the line scan shown in Fig. 2) as a function of distance from the edge of the monolayer graphene. In Figure A, the intensity profiles were plotted in linear scale to show the obvious difference in WHM of the point spread function (PSF) at lower energy loss range. While for Figure B, logarithmic scale was used in order to show the difference in the tails of the PSF. The simultaneous ADF signals and EELS signal at 95 eV in Figure B were only plotted up to 3 nm from the edge, from where the noise level dominates. This data set was collected at 60 kV with 30 mrad convergence semi-angle and 48 mrad collection semi-angle.

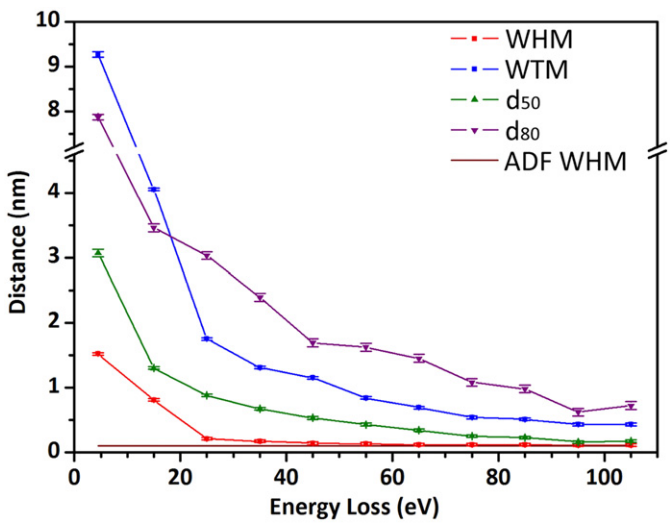

Fig. 5. Width at half maximum (WHM), width at 1/10 maximum (WTM), distance containing 50% (d_{50}) and 80% (d_{80}) of the total inelastic scattering for the EELS PSF plotted as a function of energy loss. The data set was collected at 60 kV with a 30 mrad convergence semi-angle and a 48 mrad collection semi-angle.

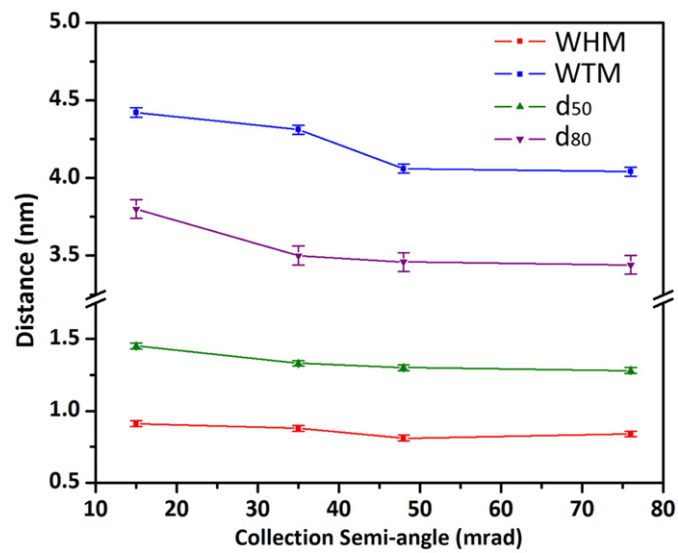

Fig. 6. WHM, WTM, d_{50} and d_{80} values obtained experimentally as a function of the collection semi-angle for the PSF for an energy loss of 15 eV. The data sets were collected at 60 kV with a 30 mrad convergence semi-angle.

collection angles smaller than the convergence angle. This observation is consistent with quantum mechanical calculations by Allen et al. [3].

To further illustrate that delocalization of inelastic electron scattering is electron-excitation mode dependent, we look at the low-loss response of graphene at ~11 eV. As shown in Fig. 7, the WHM of the PSF at 11 eV energy loss, measured from the intensity decay at the graphene edge, is about 1.23 nm, which falls in between those for the two bulk plasmon peaks (i.e. 4.5 and 15 eV) as expected. The increased delocalization is also reflected in the broadened tail of the PSF at 11 eV as compared with 16 eV (Fig. 7A). However, at the edge of the graphene layer, there is a clear increase in scattering intensity at 11 eV due to the presence of a pronounced electronic excitation mode at the graphene edge. A 4th order polynomial fitting was used to model the smooth delay of the 11 eV signal at the graphene edge, as if there were no edge enhancement. The spatial range for the edge enhancement can then be obtained by subtracting the raw data for 11 eV with this polynomial fitting. As shown in Fig. 7B, the FWHM of the edge enhancement region is estimated to be 5.6 Å. It is commonly accepted that for EELS imaging, the FWHM of the signal serves as a good criterion for determining the spatial resolution of the imaging [1,3,19]. Considering that the WHM of the PSF for 11 eV energy loss is measured at about 1.23 nm (Fig. 7B), we should not expect sub-nm resolution EELS imaging at this energy loss regime. However, the EELS image using the signal at 11 eV (Fig. 8B) clearly shows sub-nm spatial resolution of the edge state at the interface of monolayer graphene and vacuum, arising presumably either from an electronic collective excitation in the form of a one-dimensional plasmon or a one-dimensional interband transition. Our experimental results clearly indicate that the spatial resolution of EELS imaging in the low-loss regime is strongly dependent on the nature of the electronic excitations.

4. Conclusion

As aberration-corrected STEM instruments are readily available in many research labs, atomic resolution imaging and 2D core-loss EELS imaging can now be routinely performed. Atomic resolution EELS imaging at the low-loss energy regime, which provides information about the electronic structure and optical

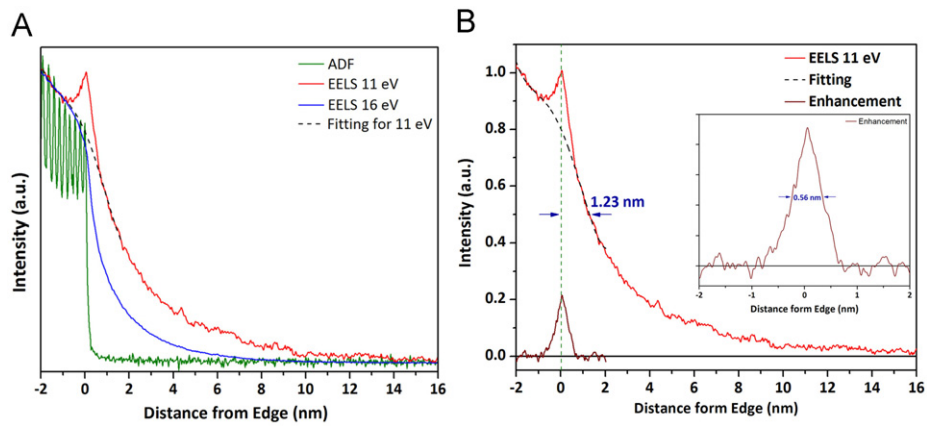

Fig. 7. Experimental measurement of inelastic scattering intensity as a function of distance from the edge of the monolayer gaphene along the line scan shown in Fig. 2. Signal enhancement at the graphene edge can be observed at an energy loss of 11 eV but not for the 16 eV energy loss. Figure B illustrates how the WHM for the PSF and the FWHM for the edge enhancement region was measured. A polynomial fit (dashed line) was used to model the smooth decay of the 11 eV signal at the graphene edge, as if there were no edge enhancement. The data set was collected at 60 kV with a 30 mrad convergence semi-angle and a 48 mrad collection semi-angle.

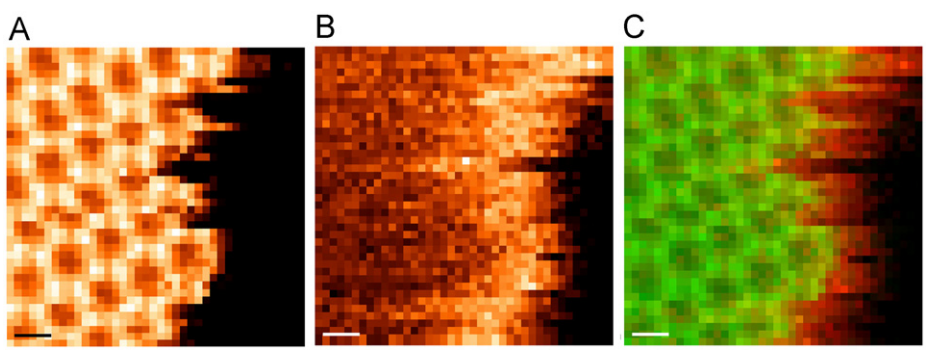

Fig. 8. Two-dimensional EELS imaging with sub-nm resolution of the low-loss response at 11 eV for an interface between monolayer graphene and vacuum. (A) ADF image collected simultaneously during spectrum imaging acquisition showing the interface between monolayer graphene and vacuum. (B) Spectrum image obtained from the raw data using the low-loss response of graphene at 11 eV. Signal enhancement at the graphene edge can be clearly mapped out with sub-nm spatial resolution even though the WHM of the inelastic scattering at this energy loss is about 1.23 nm. (C) RGB reconstructed spectrum image with ADF signal in green and plasmon signal in red. Scale bars: 0.2 nm. The data was collected at 60 kV with a 30 mrad convergence semi-angle and a 48 mrad collection semi-angle.

response of the material, seems to be the next thing to expect from the new generation of aberration corrected STEM. The question is: Can the low loss inelastic electron scattering be localized enough to be mapped out with atomic resolution?

Using a clean open edge of monolayer graphene, which provides a well-defined edge on a perfectly thin sample, we directly measure the delocalization of inelastic electron scattering at different energy loss. At energy loss higher than 25 eV where no strong characteristic excitation is present, the WHM of the PSF is only slightly worse than that of the incident electron probe, and depends weakly on the energy loss. The WHM provides a measure of the visibility of signals above the continuous background; thus suggesting that atomic resolution EELS imaging could potentially be achieved in this energy range. The increased delocalization at lower energy loss is mainly reflected in the broadened tail of the PSF, which reduces the contrast in the EELS imaging and must be taken into account for analytical work.

At lower energy losses, our results suggest that the delocalization depends not only on the energy loss, but also on the specific electron excitation modes contributing to the energy loss. For the two bulk plasmon peaks of graphene at ~4.5 and 15 eV, a drastic increase in the WHM value and significant broadening in the tail of the PSF were observed. The high degree of delocalization for the bulk plasmon signals is most likely a result of the delocalized valence states and empty states that are involved in the plasmon excitations. In contrast, at the graphene edge, we see an enhancement at ~11 eV energy loss that shows a spatial resolution of ~6 Å, even though the WHM of the PSF at this energy range, as measured from the decay of the signal away from the graphene edge, is 1.23 nm, twice greater. The sub-nm resolution at 11 eV thus suggests that the detailed nature of the specific electron excitation mode contributes to the delocalization effect in the low loss energy range, and should be included in any theoretical calculation of the response. The result also suggests that a one-dimensional collective excitation mode, either a plasmon or an inter-band transition, is produced at the edge of monolayer graphene with an excitation energy centered at ~11 eV. Finally, we anticipate that if the initial states and/or final states contributing to the energy loss are atomically localized, 2D atomic resolution EELS imaging using low loss signals could potentially be achieved.

Acknowledgments

We thank M.P. Oxley for helpful discussions and comments. This research was supported by the U.S. National Science Foundation through grant no. DMR-0938330 (WZ); Oak Ridge National

Laboratory's SHaRE User Facility (JCI), which is sponsored by the Office of Basic Energy Sciences, U.S. Department of Energy; the Office of Basic Energy Sciences, Materials Sciences and Engineering Division, U.S. Department of Energy (SJP).

References

[1] R.F. Egerton, Electron Energy-Loss Spectroscopy in the Electron Microscope, 3rd edition, Springer, New York, 2011.
[2] J.C.H. Spence, The use of characteristic-loss energy selected electron diffraction patterns for site symmetry determination, Optik 57 (1980) 451–456.
[3] L.J. Allen, S.D. Findlay, M.P. Oxley, Simulation and interpretation of images, in: S.J. Pennycook, P.D. Nellist (Eds.), Scanning Transmission Electron Microscopy: Imaging and Analysis, Springer, New York, 2011.
[4] M. Bosman, V.J. Keast, J.L. Garcia-Munoz, A.J. D'Alfonso, S.D. Findlay, L.J. Allen, Two-dimensional mapping of chemical information at atomic resolution, Physics Review Letters 90 (2007) 086102.
[5] K. Kimoto, T. Asaka, T. Nagai, M. Saito, Y. Matsui, K. Ishizuka, Element-selective imaging of atomic columns in a crystal using STEM and EELS, Nature 450 (2007) 702–704.
[6] D.A. Muller, L.F. Kourkoutis, M. Murfitt, J.H. Song, H.Y. Hwang, J. Silcox, N. Dellby, O.L. Krivanek, Atomic-scale chemical imaging of composition and bonding by aberration-corrected microscopy, Science 319 (2008) 1073–1076.
[7] M. Varela, M.P. Oxley, W. Luo, J. Tao, M. Watanabe, A.R. Lupini, S.T. Pantelides, S.J. Pennycook, Atomic-resolution imaging of oxidation states in manganites, Physics Review B 79 (2009) 085117.
[8] O.L. Krivanek, N. Dellby, M.F. Murfitt, M.F. Chisholm, T.J. Pennycook, K. Suenaga, V. Nicolosi, Gentle STEM: ADF imaging and EELS at low primary energies, Ultramicroscopy 110 (2010) 935.
[9] J. Gazquez, W. Luo, M.P. Oxley, M. Prange, M.A. Torija, M. Sharma, C. Leighton, S.T. Pantelides, S.J. Pennycook, M. Varela, Atomic-resolution imaging of spin-state superlattices in nanopockets within cobaltite thin films, Nano Letters 11 (2011) 973–976.
[10] T.J. Pennycook, M.P. Oxley, J. Garcia-Barriocanal, F.Y. Bruno, C. Leon, J. Santamaria, S.T. Pantelides, M. Varela, S.J. Pennycook, Seeing oxygen disorder in YSZ/$SrTiO_3$ colossal ionic conductor heterostructures using EELS, European Physical Journal—Applied Physics 54 (2011) 33507.
[11] M. Isaacson, J.P. Langmore, H. Rose, Determination of the non-localization of the inelastic scattering of electrons by electron microscopy, Optik 41 (1974) 92–96.
[12] H. Rose, Image formation by inelastically scattered electrons in electron microscopy, Optik 45 (1976) 139–158.
[13] H. Rose, Image formation by inelastically scattered electrons in electron microscopy II, Optik 45 (1976) 187–208.
[14] H. Kohl, H. Rose, Theory of image formation by inelastically scattered electrons in the electron microscope, Advances in Electronics and Electron Physics 65 (1985) 175–200.
[15] P.E. Batson, A new surface plasmon resonance in clusters of small aluminum spheres, Ultramicroscopy 9 (1982) 277–282.
[16] M. Scheinfein, A. Muray, M. Isaacson, Electron energy loss spectroscopy across a metal-insulator interface at sub-nanometer spatial resolution, Ultramicroscopy 16 (1985) 233–240.
[17] M. Scheinfein, M. Isaacson, Electronic and chemical analysis of fluoride interface structures at subnanometer spatial resolution, Journal of Vacuum Science and Technology B 4 (1986) 326–332.
[18] M. Schenner, P. Schattschneider, Spatial resolution in selected-area EELS, Ultramicroscopy 55 (1994) 31–41.
[19] D.A. Muller, J. Silcox, Delocalization in inelastic scattering, Ultramicroscopy 59 (1995) 195–213.
[20] K. van Benthem, R.H. French, W. Sigle, C. Elsasser, M. Ruhle, Valence electron energy loss study of Fe-doped $SrTiO_3$ and a $\sum 13$ boundary: electronic structure and dispersion forces, Ultramicroscopy 86 (2001) 303–318.
[21] E.C. Cosgriff, M.P. Oxley, L.J. Allen, S.J. Pennycook, The spatial resolution of imaging using core-loss spectroscopy in the scanning transmission electron microscope, Ultramicroscopy 102 (2005) 317–326.
[22] H.L. Xin, L.F. Kourkoutis, J.A. Mundy, H. Zheng, D.A. Muller, Atomic-scale EELS maps: it's not resolution, but contrast, Microscopy and Microanalysis 16 (2) (2010) 242–243.
[23] R. Erni, N.D. Browning, Valence electron energy-loss spectroscopy in monochromated scanning transmission electron microscopy, Ultramicroscopy 104 (2005) 176–192.
[24] M.P. Oxley, E.C. Cosgriff, L.J. Allen, Nonlocality in imaging, Physics Review Letters 94 (2005) 203906.
[25] M.H. Gass, et al., Free-standing graphene at atomic resolution, Nature Nanotechnology 3 (2008) 676–681.